

Twentieth International Specialty Conference on Cold-Formed Steel Structures  
Saint Louis, Missouri, USA, November 3 & 4, 2010

**Buckling analysis of cold-formed steel members with general  
boundary conditions using CUFSM:  
conventional and constrained finite strip methods**

Z. Li<sup>1</sup> and B. W. Schafer<sup>2</sup>

**Abstract**

The objective of this paper is to provide the theoretical background and illustrative examples for elastic buckling analysis of cold-formed steel members with general boundary conditions as implemented in the forthcoming update to CUFSM. CUFSM is an open source finite strip elastic stability analysis program freely distributed by the senior author. Although the finite strip method presents a general methodology, the conventional implementation (e.g. CUFSM v 3.13 or earlier) employs only simply-supported boundary conditions. In this paper, utilizing specially selected longitudinal shape functions, the conventional finite strip method is extended to general boundary conditions, including the conventional case: simply-simply supported, as well as: clamped-clamped, clamped-simply supported, clamped-free, and clamped-guided. The solution remains semi-analytical as the elastic and geometric stiffness matrices are derived in a general form with only specific integrals depending on the boundary conditions. An example of the stability solution is provided. The selection of longitudinal terms to be included in the analysis is discussed in terms of balancing accuracy with computational efficiency. Also herein, the constrained finite strip method is extended to general boundary conditions. Both modal decomposition and identification can be carried out based on the new bases developed for the constrained finite strip method, and illustrative examples are provided. This extension of CUFSM is intended to aid the implementation of the direct strength method to the case of general boundary conditions.

**Keywords:** Finite strip method, constrained finite strip method, boundary conditions, elastic buckling analysis, CUFSM

---

<sup>1</sup> Ph.D. Candidate, Johns Hopkins Univ., Baltimore, MD, [lizhanjie@jhu.edu](mailto:lizhanjie@jhu.edu)

<sup>2</sup> Professor, Johns Hopkins Univ., Baltimore, MD, [schafer@jhu.edu](mailto:schafer@jhu.edu)

## Introduction

Cold-formed steel members are thin, light and economically efficient. However, this efficiency comes with complication. Engineers must account for cross section instability (i.e., local and distortional) in addition to global buckling (Euler) of the member. Numerical solutions, such as the finite strip method (FSM), are particularly important for addressing this complexity as they take into consideration the inter-element interaction and as a result provide far more accurate solutions for local and distortional buckling than typical hand formulas.

Conventional FSM, e.g., CUFSM [1], freely available from the senior author's website ([www.ce.jhu.edu/bschafer/cufsm](http://www.ce.jhu.edu/bschafer/cufsm)), provides a method to examine all the instabilities in a cold-formed steel member under uniform longitudinal stresses (axial, bending, warping torsion, or combinations thereof). Additionally, the newly developed constrained finite strip method (cFSM) is implemented in CUFSM. When the signature curve of the conventional FSM is not able to provide distinct minima that correspond to local and distortional buckling mode [2], cFSM becomes essential for accurately determining the buckling modes and greatly eases and generalizes implementation in new design methods such as the Direct Strength Method (DSM) [3]. However, existing CUFSM and cFSM implementations are applicable to only simply supported end boundary conditions.

Recently, extensions of the conventional FSM and cFSM to general end boundary conditions, namely: simple-simple (S-S), clamped-clamped (C-C), simple-clamped (S-C), clamped-free (C-F), and clamped-guided (C-G), have been explored by Li and Schafer [4, 5]. Specially selected longitudinal shape functions are employed to represent the specified boundary condition [4, 6] as follows:

$$\text{simple-simple, } Y_{[m]} = \sin(m\pi y/a) \quad (1)$$

$$\text{clamped-clamped, } Y_{[m]} = \sin(m\pi y/a)\sin(\pi y/a) \quad (2)$$

$$\text{simple-clamped, } Y_{[m]} = \sin[(m+1)\pi y/a] + (m+1/m)\sin(m\pi y/a) \quad (3)$$

$$\text{clamped-free, } Y_{[m]} = 1 - \cos[(m-1/2)\pi y/a] \quad (4)$$

$$\text{clamped-guided, } Y_{[m]} = \sin[(m-1/2)\pi y/a]\sin(\pi y/2/a) \quad (5)$$

where,  $m$  indicates the longitudinal term to be summed to form the displacement field. These shape functions have been implemented into a new version of CUFSM for both conventional and constrained FSM (cFSM). To provide the theoretical basis of this solution the underlying elastic and geometric stiffness matrices are briefly derived and presented. In addition, stability solutions for general boundary conditions are provided against the typical signature curve to

illustrate their coherent relationship. The underlying theory and procedure of cFSM for general boundary conditions is provided along with related examples. Finally, FSM and cFSM for general end boundary conditions are employed for use with the DSM design procedure. The coupling between longitudinal terms for non-simply supported boundary conditions creates complications and new procedures are suggested.

### Conventional Finite Strip Method

A typical strip for a thin-walled member is depicted in Figure 1, along with the degrees of freedom ( $u_1, v_1, w_1, \theta_1$ , etc., for the  $m=1$  longitudinal term) applied end tractions ( $T_1, T_2$ ) and the global/member ( $X, Y, Z$ ) and local/strip ( $x, y, z$ ) coordinate systems.

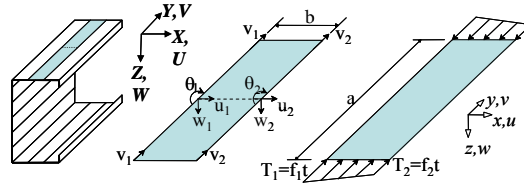


Figure 1 Coordinates, Degree of Freedom, and loads of a typical strip

The  $u$ ,  $v$  and  $w$  displacement fields are approximated with shape functions and nodal displacements. These displacement fields are summed for each longitudinal term  $m$ , up to  $q$ , specifically:

$$u = \sum_{m=1}^q \left[ \left(1 - \frac{x}{b}\right) \frac{x}{b} \right] \begin{Bmatrix} u_{1[m]} \\ u_{2[m]} \end{Bmatrix} Y_{[m]}, \quad v = \sum_{m=1}^q \left[ \left(1 - \frac{x}{b}\right) \frac{x}{b} \right] \begin{Bmatrix} v_{1[m]} \\ v_{2[m]} \end{Bmatrix} Y'_{[m]} \frac{a}{\mu_{[m]}} \quad (6)$$

$$w = \sum_{m=1}^q \left[ 1 - \frac{3x^2}{b^2} + \frac{2x^3}{b^3} \quad x \left(1 - \frac{2x}{b} + \frac{x^2}{b^2}\right) \quad \frac{3x^2}{b^2} - \frac{2x^3}{b^3} \quad x \left(\frac{x^2}{b^2} - \frac{x}{b}\right) \right] Y_{[m]} d_{w[m]} \quad (7)$$

where  $d_{w[m]} = [w_{1[m]} \quad \theta_{1[m]} \quad w_{2[m]} \quad \theta_{2[m]}]$  and  $\mu_{[m]} = m\pi$ . The shape function of the strip in the transverse direction is the same as a classical beam finite element, while in the longitudinal direction,  $Y_{[m]}$ , is employed with trigonometric functions as shown in Eq. 's (1)-(5).

### Elastic and Geometric stiffness matrices

For the elastic stiffness matrices the strain in the strip consists of two portions: membrane and bending. The membrane strains are at the mid-plane of the strip and governed by plane stress assumptions. The bending strains follow Kirchhoff thin plate theory and are zero at the mid-plane, and a function of  $w$  alone. For

each strip, the elastic stiffness matrix  $k_e$  can be formulated through the internal energy integration, where stress is connected to strain by an orthotropic plane stress constitutive relation. See [1] and [4] for full derivation. Matrix  $k_e^{[mn]}$  corresponding to longitudinal terms  $m$  and  $n$  is one block elastic stiffness matrix of the full elastic stiffness matrix  $k_e$ , which can be separated for membrane ( $M$ ) and bending ( $B$ ),

$$k_e^{[mn]} = \begin{bmatrix} k_{eM}^{[mn]} & \cdot \\ \cdot & k_{eB}^{[mn]} \end{bmatrix} \quad (8)$$

The closed-form expressions for the membrane,  $k_{eM}^{[mn]}$ , and the bending,  $k_{eB}^{[mn]}$ , elastic stiffness matrices are provided as follows:

$$k_{eM}^{[mn]} = t \begin{bmatrix} \left( \frac{E_1 I_1}{b} + \frac{G b I_5}{3} \right) & \left( -\frac{E_2 v_x I_3}{2c_2} - \frac{G I_5}{2c_2} \right) & \left( -\frac{E_1 I_1}{b} + \frac{G b I_5}{6} \right) & \left( -\frac{E_2 v_x I_3}{2c_2} + \frac{G I_5}{2c_2} \right) \\ \left( -\frac{E_2 v_x I_3}{2c_1} - \frac{G I_5}{2c_1} \right) & \left( \frac{E_2 b I_4}{3c_1 c_2} + \frac{G I_5}{b c_1 c_2} \right) & \left( \frac{E_2 v_x I_3}{2c_1} - \frac{G I_5}{2c_1} \right) & \left( \frac{E_2 b I_4}{6c_1 c_2} - \frac{G I_5}{b c_1 c_2} \right) \\ \left( -\frac{E_1 I_1}{b} + \frac{G b I_5}{6} \right) & \left( \frac{E_2 v_x I_3}{2c_2} - \frac{G I_5}{2c_2} \right) & \left( \frac{E_1 I_1}{b} + \frac{G b I_5}{3} \right) & \left( \frac{E_2 v_x I_3}{2c_2} + \frac{G I_5}{2c_2} \right) \\ \left( -\frac{E_2 v_x I_3}{2c_1} + \frac{G I_5}{2c_1} \right) & \left( \frac{E_2 b I_4}{6c_1 c_2} - \frac{G I_5}{b c_1 c_2} \right) & \left( \frac{E_2 v_x I_3}{2c_1} + \frac{G I_5}{2c_1} \right) & \left( \frac{E_2 b I_4}{3c_1 c_2} + \frac{G I_5}{b c_1 c_2} \right) \end{bmatrix} \quad (9)$$

$$k_{eB}^{[mn]} = \frac{1}{420b^3} \begin{bmatrix} \begin{pmatrix} 5040D_x I_1 - 504b^2 D_x I_2 \\ -504b^2 D_x I_3 + 156b^4 D_x I_4 \\ + 2016b^2 D_y I_5 \end{pmatrix} & \begin{pmatrix} 2520bD_x I_1 - 462b^3 D_x I_2 \\ -42b^3 D_x I_3 + 22b^5 D_x I_4 \\ + 168b^3 D_y I_5 \end{pmatrix} & \begin{pmatrix} -5040D_x I_1 + 504b^2 D_x I_2 \\ + 504b^2 D_x I_3 + 54b^4 D_x I_4 \\ - 2016b^2 D_y I_5 \end{pmatrix} & \begin{pmatrix} 2520bD_x I_1 - 42b^3 D_x I_2 \\ -42b^3 D_x I_3 - 13b^5 D_x I_4 \\ + 168b^3 D_y I_5 \end{pmatrix} \\ \begin{pmatrix} 2520bD_x I_1 - 462b^3 D_x I_2 \\ -42b^3 D_x I_3 + 22b^5 D_x I_4 \\ + 168b^3 D_y I_5 \end{pmatrix} & \begin{pmatrix} 1680b^2 D_x I_1 - 56b^4 D_x I_2 \\ -56b^4 D_x I_3 + 4b^6 D_x I_4 \\ + 224b^4 D_y I_5 \end{pmatrix} & \begin{pmatrix} -2520bD_x I_1 + 42b^3 D_x I_2 \\ + 42b^3 D_x I_3 + 13b^5 D_x I_4 \\ - 168b^3 D_y I_5 \end{pmatrix} & \begin{pmatrix} 840b^2 D_x I_1 + 14b^4 D_x I_2 \\ + 14b^4 D_x I_3 - 3b^6 D_x I_4 \\ - 56b^4 D_y I_5 \end{pmatrix} \\ \begin{pmatrix} -5040D_x I_1 + 504b^2 D_x I_2 \\ + 504b^2 D_x I_3 + 54b^4 D_x I_4 \\ - 2016b^2 D_y I_5 \end{pmatrix} & \begin{pmatrix} -2520bD_x I_1 + 42b^3 D_x I_2 \\ + 42b^3 D_x I_3 + 13b^5 D_x I_4 \\ - 168b^3 D_y I_5 \end{pmatrix} & \begin{pmatrix} 5040D_x I_1 - 504b^2 D_x I_2 \\ -504b^2 D_x I_3 + 156b^4 D_x I_4 \\ + 2016b^2 D_y I_5 \end{pmatrix} & \begin{pmatrix} -2520bD_x I_1 + 462b^3 D_x I_2 \\ + 42b^3 D_x I_3 - 22b^5 D_x I_4 \\ - 168b^3 D_y I_5 \end{pmatrix} \\ \begin{pmatrix} 2520bD_x I_1 - 42b^3 D_x I_2 \\ -42b^3 D_x I_3 - 13b^5 D_x I_4 \\ + 168b^3 D_y I_5 \end{pmatrix} & \begin{pmatrix} 840b^2 D_x I_1 + 14b^4 D_x I_2 \\ + 14b^4 D_x I_3 - 3b^6 D_x I_4 \\ - 56b^4 D_y I_5 \end{pmatrix} & \begin{pmatrix} -2520bD_x I_1 + 462b^3 D_x I_2 \\ + 42b^3 D_x I_3 + 13b^5 D_x I_4 \\ - 168b^3 D_y I_5 \end{pmatrix} & \begin{pmatrix} 1680b^2 D_x I_1 - 56b^4 D_x I_2 \\ -56b^4 D_x I_3 + 4b^6 D_x I_4 \\ + 224b^4 D_y I_5 \end{pmatrix} \end{bmatrix} \quad (10)$$

where  $c_1 = \frac{m\pi}{a}$   $c_2 = \frac{n\pi}{a}$   $I_1 = \int_0^a Y_{[m]} Y_{[n]} dy$   $I_2 = \int_0^a Y_{[m]}'' Y_{[n]} dy$   $I_3 = \int_0^a Y_{[m]} Y_{[n]}'' dy$   $I_4 = \int_0^a Y_{[m]}'' Y_{[n]}'' dy$

$$I_5 = \int_0^a Y_{[m]}' Y_{[n]}' dy \quad [D_M] = \begin{bmatrix} E_1 & v_x E_2 & 0 \\ v_y E_1 & E_2 & 0 \\ 0 & 0 & G \end{bmatrix} \quad E_1 = \frac{E_x}{1 - v_x v_y} \quad E_2 = \frac{E_y}{1 - v_x v_y} \quad [D_B] = \begin{bmatrix} D_x & D_1 & 0 \\ D_1 & D_y & 0 \\ 0 & 0 & D_{xy} \end{bmatrix}$$

$$D_x = \frac{E_x t^3}{12(1 - v_x v_y)} \quad D_y = \frac{E_y t^3}{12(1 - v_x v_y)} \quad D_1 = \frac{v_y E_x t^3}{12(1 - v_x v_y)} = \frac{v_x E_y t^3}{12(1 - v_x v_y)} \quad D_{xy} = \frac{G t^3}{12}$$

The geometric stiffness matrix is determined by examining the potential work created as the plate shortens, e.g., due to out-of-plane bending (or the Lagrangian strain terms), allows the geometric stiffness matrix  $k_g$  to be formulated as well (see complete derivation in [1, 4]). Similar to the elastic stiffness matrix,  $k_g^{[mn]}$  corresponding to longitudinal terms  $m$  and  $n$  is broken

into membrane,  $k_{gM}^{[mn]}$  and bending,  $k_{gB}^{[mn]}$ , in the similar format of Eq. (8). The explicit expressions are given below:

$$k_{gM}^{[mn]} = \begin{bmatrix} \frac{(3T_1 + T_2)bI_5}{12} & 0 & \frac{(T_1 + T_2)bI_5}{12} & 0 \\ & \frac{(3T_1 + T_2)ba^2I_4}{12\mu_m\mu_n} & 0 & \frac{(T_1 + T_2)ba^2I_4}{12\mu_m\mu_n} \\ & & \frac{(T_1 + 3T_2)bI_5}{12} & 0 \\ \text{symmetric} & & & \frac{(T_1 + 3T_2)ba^2I_4}{12\mu_m\mu_n} \end{bmatrix} \quad (11)$$

$$k_{gB}^{[mn]} = \begin{bmatrix} \frac{(10T_1 + 3T_2)bI_5}{35} & \frac{(15T_1 + 7T_2)b^2I_5}{420} & \frac{9(T_1 + T_2)bI_5}{140} & -\frac{(7T_1 + 6T_2)b^2I_5}{420} \\ & \frac{(5T_1 + 3T_2)b^3I_5}{840} & \frac{(6T_1 + 7T_2)b^2I_5}{420} & -\frac{(T_1 + T_2)b^3I_5}{280} \\ & & \frac{(3T_1 + 10T_2)bI_5}{35} & -\frac{(7T_1 + 15T_2)b^2I_5}{420} \\ \text{symmetric} & & & \frac{(3T_1 + 5T_2)b^3I_5}{840} \end{bmatrix} \quad (12)$$

where  $\mu_m = m\pi$ ;  $\mu_n = n\pi$ ;  $I_4 = \int_0^a Y_{[m]}'' Y_{[n]}'' dy$ ;  $I_5 = \int_0^a Y_{[m]}' Y_{[n]}' dy$

The full elastic stiffness matrix  $k_e$  and geometric stiffness matrix  $k_g$  can be expressed as:

$$k_e = [k_e^{[mn]}]_{q \times q} \quad \text{and} \quad k_g = [k_g^{[mn]}]_{q \times q} \quad (13)$$

where each  $k_e^{[mn]}$  and  $k_g^{[mn]}$  submatrices are  $8 \times 8$  and  $q^2$  such submatrices exist.

Note,  $I_1$  through  $I_5$  are zero when  $m \neq n$  for the simple-simple (S-S) boundary conditions leaving only a diagonal set of submatrices in  $k_e$  and  $k_g$ . It is this efficiency that leads to the attractive nature of the classical solution and the universality of the buckling half-wavelength vs. buckling load curve (signature curve) for the S-S boundary conditions. For all other boundary conditions  $k_e$  and  $k_g$  have non-zero submatrices off the main diagonal and interaction of buckling modes of different half-wavelengths (or longitudinal terms) occur and the signature curve loses its special significance. In essence, for all boundary conditions other than S-S, FSM has the same identification problems as finite element method (FEM), unless other tools such as the constrained FSM are implemented.

#### Assembly and Stability solutions

After necessary transformation from local to global coordinates based on the strip orientation and appropriate assembly over all the strips, the global elastic ( $K_e$ ) and geometric ( $K_g$ ) stiffness matrices can be obtained. See complete details in [1] and [4]. For a given distribution of edge tractions on a member the

geometric stiffness matrix scales linearly, resulting in the elastic buckling problem:

$$K_e \Phi = \Lambda K_g \Phi \quad (14)$$

where,  $\Lambda$  is a diagonal matrix containing the eigenvalues (buckling loads) and  $\Phi$  is a fully populated matrix corresponding to the eigenmodes (buckling modes) in its columns. Validation of the conventional FSM solution may be found in [4].

#### **Signature curve and FSM solution of general boundary conditions**

To illustrate the stability solution for general boundary conditions and reveal its relationship with the popularized “signature curve” the stability solutions for a 400S162-68 SSMA stud section [7] under major-axis bending are provided for simple (*S-S*) and clamped (*C-C*) boundary conditions in Figure 2. Note, the signature curve is a special case of the *S-S* FSM solution where only a single longitudinal term (i.e.,  $m=1$ ) is employed. FSM solutions for *S-S* boundary conditions for any  $m$  are independent due to the resulting orthogonality in  $K_e$  and  $K_g$  and further the buckling load for any  $m$  may be found by performing the solution for  $m=1$  at a length equal to  $a/m$ . As a result, it has become conventional to express FSM solutions of *S-S* boundary conditions in terms of the first buckling load over a series of lengths as opposed to FEM solutions where typically a model is solved for many buckling loads at a single length by examining higher mode solutions [8].

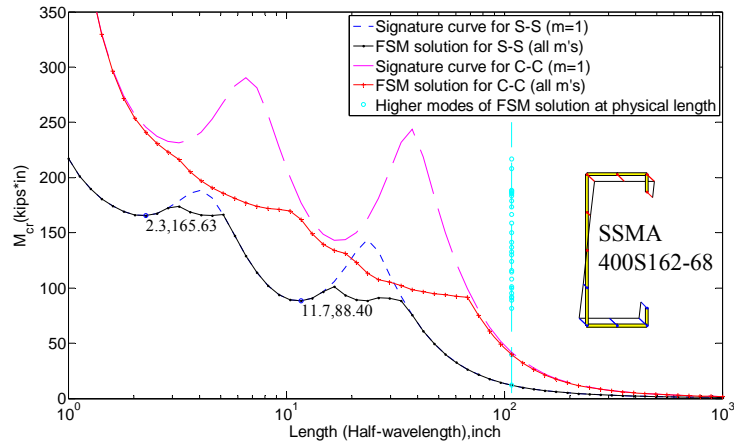


Figure 2 Signature curve and FSM solution for general boundary conditions

For FSM with non simply-supported boundary conditions the orthogonality is lost, and thus the special meaning of the signature curve (an  $m=1$  solution with

varying length  $a$ ) is lost, as shown in Figure 2. Given that many longitudinal ( $m$ ) terms are used the solution should be interpreted as a function of physical length, as opposed to half-wavelength. In fact, the FSM solution captures the potential interaction of longitudinal terms, and it would be equally valid to use the FEM approach and examine higher mode solutions at a given length (e.g., at  $L \sim 100$  in. as shown), instead of varying  $a$  as shown in Figure 2.

### Longitudinal terms

Although the signature curve is ineffective for non simply-supported boundary conditions, the buckling nature in terms of the inherent half-wavelengths of local, distortional, and global buckling from the signature curve still provide useful information. For problem size and computational efficiency the total number of longitudinal terms included in the analysis should be minimized. Accordingly, longitudinal terms for the physical length ( $L$ ) to be analyzed should be wisely selected so that higher modes reported from the FSM solution consist of all the three modes (local, distortional and global). Studies in [4] show that given the simply supported half-wavelengths of local ( $L_{crl}$ ), distortional ( $L_{crd}$ ), and global ( $L_{cre}$ ) buckling these represent the three regimes for  $m$  of greatest interest, i.e.  $m$  near  $L/L_{crl}$ ,  $L/L_{crd}$ , and  $L/L_{cre}$ . Note, usually,  $L_{cre}$  is the physical length, thus 1, 2, and 3 are chosen around  $L/L_{cre}$ , and 7 longitudinal terms chosen around  $L/L_{crl}$  and  $L/L_{crd}$  to include relevant potential couplings.

The critical buckling moments of the first 10 modes at  $L=108$  in. (see Figure 2) are listed in Table 1 for both  $S-S$  and  $C-C$  boundary conditions using the suggested longitudinal terms. For the  $S-S$  case, modes 1, 4 and 10 are the global, distortional, and local buckling modes, respectively, and match exactly the signature curve. For the  $C-C$  case, critical moments have a negligible difference compared with the solution with all longitudinal terms included, e.g., mode 3  $M_{crd}$  is 0.05% lower with all terms. The difference of the participation of longitudinal terms is illustrated for the 3<sup>rd</sup> mode in Figure 3.

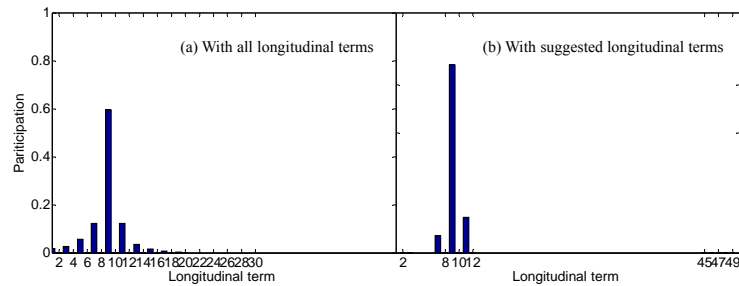






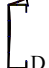
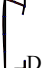




Figure 3 Participations of longitudinal terms for 3<sup>rd</sup> mode of FSM solution

Table 1 Higher modes of FSM solution for *S-S* and *C-C* (kips-in)

Higher modes	$M_{cr}$ of FSM solution for <i>S-S</i>		$M_{cr}$ of FSM solution for <i>C-C</i>	
1	11.94		40.90	
2	39.47		78.63	
3	81.58		89.86	
4	88.65		90.01	
... Higher order D modes			... Higher order D modes	
10	165.53		165.58	

### Constrained Finite Strip Method

The concept and theory of the constrained FSM (*cFSM*) for *S-S* boundary conditions is well established [1, 9-11] and at its heart employs the same mechanical assumptions of the deformation modes utilized in Generalized Beam Theory (GBT) [12, 13]. In *cFSM*, the mechanical assumptions provide a means to categorize any deformation, including buckling modes into global (G), distortional (D), local (L), and other (O, or shear and transverse extension--ST) deformation spaces. The key feature of *cFSM* is that the general displacement field  $d$  may be constrained to any “modal” deformation space,  $M$ , via:

$$d = R_M d_M \quad (15)$$

where  $R_M$  is the constraint matrix for the selected modal space(s) (*G*, *D*, *L*, *O* (*ST*) or any combination thereof) and  $d_M$  is the resulting deformations within that space.

Recently, the authors extended FSM and *cFSM* to the case of general end boundary conditions [4, 5] and this paper summarizes that work as implemented in CUFSM. *cFSM* provides the ability to perform modal decomposition of stability solutions as well as quantitative modal identification. Extension to general boundary conditions is an important step towards *cFSM*’s application in general purpose design situations.



### ***Buckling mode definition***

The essential feature of *cFSM* is the separation of general deformations into those deformations consistent with *G*, *D*, *L*, and *ST/O* deformation spaces. The deformation spaces are defined by the mechanical assumptions inherent within each space. The criteria are provided below in Table 2 and implemented for each space, as is typical in the *cFSM* literature [1, 4, 5, 9-11].

Table 2 Mechanical criteria of mode definition

Mechanical criteria	G	D	L	ST/O
$\gamma_{xy} = 0$ , $\varepsilon_x = 0$ , $v$ is linear (Vlasov's hypotheses)	Yes	Yes	Yes	No
$\varepsilon_y \neq 0$ (longitudinal warping)	Yes	Yes	No	-
$\kappa_y = 0$ (undistorted section)	Yes	No	-	-

### ***Base definition***

Although Table 2 defines the deformation spaces, there are some subtleties in the implementation which do influence the resulting modal decomposition or identification. Full details of the basis definitions are provided in [5] and a summary of the bases utilized in CUFSM's implementation of *cFSM* are provided in Table 3. The simplest application of the Table 3 definitions are embodied in the "Natural basis" which is defined by explicitly following the mechanical criteria (see [4]). The natural basis, which separates the deformations into the *G*, *D*, *L*, *O/ST* spaces may be transformed to a true "modal" basis (similar to GBT) by performing an auxiliary eigen problem within each space either for a unit axial stress, or for the actual applied stresses. For non-simply supported boundary conditions due to the loss of orthogonality of the stiffness matrices between longitudinal terms, whether the constrained eigenvalue problem is solved inside each longitudinal term or over all the longitudinal terms results in the uncoupled and coupled bases, respectively. Finally, two alternatives exist for defining the *O/ST* space. Either the *O* space can be built up as the union of the shear and transverse extensions (generally preferred) or the space may be defined as the null of the GDL subspace, either with respect to elastic stiffness matrix  $K_e$  ( ${}^eR_O$ ), geometric stiffness matrix  $K_g$  ( ${}^gR_O$ ), or in vector sense ( ${}^vR_O$ ) as detailed in [5].

Also, note, for the purpose of performing modal identification the base vectors in the basis have to be appropriately normalized. Normalization can be done in various ways. Three options are available and each column  $\varphi_i$  in bases must satisfy the following condition: (1) vector norm  $\|\varphi_i\|=1$ ; (2) strain energy norm  $\sqrt{\varphi_i^T K_e \varphi_i}=1$ ; and (3) work norm  $\sqrt{\varphi_i^T K_g \varphi_i}=1$ .

Table 3 Summary of defined bases

Subspaces	Orthogonalization in the subspace				
	Natural basis (not orthogonal)	Modal basis (orthogonal)			
		Axial uniform force		Applied force	
	Uncoupled basis <sup>(c)</sup>	Uncouple basis	Coupled basis	Uncouple basis	Coupled basis
GD	$\bar{R}_{GD}$	$[\bar{R}_{GD}]_m$	$\bar{R}_{GD}$	$[\bar{R}_{GD}]_m$	$\bar{R}_{GD}$
G	$\bar{R}_G^{(a)}$	$[\bar{R}_G]_m$	$\bar{R}_G$	$[\bar{R}_G]_m$	$\bar{R}_G$
D	$\bar{R}_D$	$[\bar{R}_D]_m$	$\bar{R}_D$	$[\bar{R}_D]_m$	$\bar{R}_D$
L	$\bar{R}_L$	$[\bar{R}_L]_m$	$\bar{R}_L$	$[\bar{R}_L]_m$	$\bar{R}_L$
ST/O	Shear + Trans. ext. <sup>(b)</sup> $R_{ST} = R_S \cup R_T$ Null of GDL $[R_O]_m = [{}^e R_O]_m \text{ or } [{}^s R_O]_m \text{ or } [{}^v R_O]_m$	$[\bar{R}_S]_m \cup [\bar{R}_T]_m \text{ or } [{}^e \bar{R}_O]_m \text{ or } [{}^s \bar{R}_O]_m \text{ or } [{}^v \bar{R}_O]_m$	$\bar{R}_S \cup \bar{R}_T \text{ or } {}^e \bar{R}_O \text{ or } {}^s \bar{R}_O \text{ or } {}^v \bar{R}_O$	$[\bar{R}_S]_m \cup [\bar{R}_T]_m \text{ or } [{}^e \bar{R}_O]_m \text{ or } [{}^s \bar{R}_O]_m \text{ or } [{}^v \bar{R}_O]_m$	$\bar{R}_S \cup \bar{R}_T \text{ or } {}^e \bar{R}_O \text{ or } {}^s \bar{R}_O \text{ or } {}^v \bar{R}_O$

- (a) G modes may be defined about principle axes or about geometric axes. Also pure torsion mode does not have to be about shear center, though CUFSM (and GBT) does choose to do this.  
(b) S and T may be formed from strip-wise shear and transverse extension, e.g. +1,-1 for  $v$  in a strip, or +1,0 for  $v$  in a strip leading to different S and T spaces.  
(c) Uncoupled basis means the null space of GDL or the orthogonalization is performed inside each longitudinal term  $m$ . The resulted basis is a block diagonal matrix. Coupled natural basis refers to  $R_O = {}^e R_O \text{ or } {}^s R_O \text{ or } {}^v R_O$  while GDL spaces are the same.

### Modal decomposition

The constrained eigenvalue problem may be expressed by introducing Eq. (15) into the FSM eigenvalue problem for mode or modes  $M$  as:

$$K_{e,M} \Phi_M = \Lambda_M K_{g,M} \Phi_M \quad (16)$$

where,  $K_{e,M}$  and  $K_{g,M}$  are the elastic and geometric stiffness matrix of the constrained FSM problem, respectively, and defined as  $K_{e,M} = R_M^T K_e R_M$  and  $K_{g,M} = R_M^T K_g R_M$ ,  $\Lambda_M$  is a diagonal matrix containing the eigenvalues for the given mode or modes, and  $\Phi_M$  is the matrix of corresponding modes in its columns.

To illustrate the capability of cFSM for general boundary conditions, the  $G$ ,  $D$ , and  $L$  modes are decomposed from the FSM solution using the natural basis (ST) of Table 3 and the critical moments are plotted in Figure 4 against the FSM solution for the 400S162-68 SSMA stud section under major-axis bending with C-C boundary conditions. The longitudinal terms employed are the previously recommended terms. In general, the results are consistent with the observations in previous cFSM analyses for S-S boundary conditions.

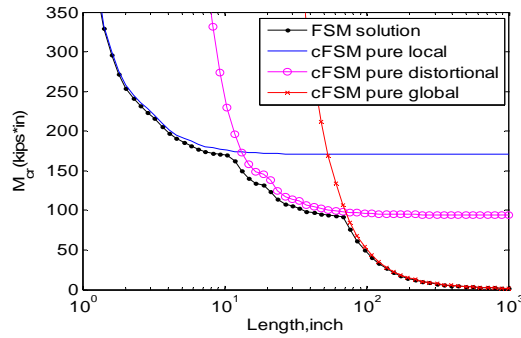


Figure 4 Modal decomposition of cFSM

Modal decomposition may also be used to search the participation of longitudinal terms for pure local and distortional buckling, and then use these longitudinal terms to force the member to buckle in local or distortional buckling mode as described in the application with DSM section at the end of this paper.

### Modal Identification

Using the defined *c*FSM bases, natural or modal, any nodal displacement vector, *d*, (deformed shape or buckling mode) may be transformed into the basis spanned by the buckling classes, via

$$c = R^{-1}d \quad (17)$$

where the coefficients in *c* represent the contribution to a given column of basis *R*. The participation of each mode class is calculated as:

$$p_M = \|c_M\|_2 / \sum_{M=G,D,L,ST/O} \|c_M\|_2 \quad (18)$$

where *c<sub>M</sub>* is column vectors of the contribution coefficients of each mode class (G, D, L, ST/O) in *c*. Eq. (19) uses the L<sup>2</sup> norm to calculate the participation of each mode class other than the absolute sum as previously used. The attraction of formal identification of the buckling modes is not just a theoretical one, as design methods such as the DSM directly utilize this information to select buckling modes and then predict ultimate strength.

To illustrate the capacity of modal identification of *c*FSM, modal participations for the higher modes of Table 1 are provided in Table 4. The basis employed is the uncoupled axial modal basis (ST) with vector norm. The classification of buckling modes (G, D, L) provide in Table 1 is completed empirically, simply by visualizing the 2D (or 3D) buckling mode. That highly subjective process can be replaced by the quantitative results of Table 4. For example the 9<sup>th</sup> mode (Figure 5) when using visual identification only may credibly be identified as distortional, but *c*FSM modal identification shows it to be dominated by global deformations with only a modest distortional contribution.

Table 4 Modal classification of higher modes of FSM solution

Higher modes	<i>M<sub>cr</sub></i>	Participation (%)			
		G	D	L	O
1	40.90	98.3	1.6	0.0	0.0
2	78.63	92.0	7.7	0.2	0.1
3	89.86	4.0	92.4	3.4	0.2
4	90.01	3.8	91.8	4.1	0.2
5	94.60	3.9	90.8	5.1	0.2
6	94.78	5.1	91.4	3.3	0.2
7	102.02	3.6	91.1	5.0	0.3
8	106.17	6.3	90.6	2.9	0.2
9	140.69	82.0	17.5	0.4	0.1
10	165.58	0.8	6.5	91.9	0.8
11	165.58	0.8	6.4	92.0	0.8
12	165.75	0.8	6.4	92.0	0.8



Figure 5 2D buckling shapes of 9<sup>th</sup> mode of FSM solution

### Application with Direct Strength Method

Together with the Direct Strength Method (DSM), an FSM solution can prove to be a powerful tool in member design. FSM application for *S-S* boundary conditions, through the signature curve, has been well studied while the application for non-simply boundary condition is still a work in progress. However, basic ideas for non-simply supported boundary conditions are explored here for the intention of developing consensus.

#### Application for simply supported boundary condition

Traditionally, the two local minima and the descending branch at longer lengths in the signature curve provide the necessary information for the local, distortional, and global buckling loads for design [1, 14-15]. However, studies on SSMA sections [2] demonstrate that the signature curve often fails to uniquely identify the modes, as illustrated in Figure 6. Although *c*FSM can uniquely identify the buckling modes, two basic issues remain: (1) DSM's strength expressions are calibrated to the conventional FSM minima instead of pure mode solutions from *c*FSM (which are generally a few percent higher), and (2) *c*FSM can not handle rounded corners. To address these issues a two-step procedure has been adopted for determining the elastic buckling loads and moments. First, in step 1, the analyst develops a rounded corner model of the section and runs a conventional FSM model. If unique minima exist the analysis is complete. If not, step 2 is completed where: the analyst develops a straight-line model of the section and runs constrained FSM pure mode solutions for local and distortional, only for the purpose of determining the length ( $L_{cr}$ ) at which the modes occur. The elastic buckling load (or moment) is determined from the conventional FSM with round corners, Step 1 model, at the  $L_{cr}$  identified in the Step 2 model. A shorthand for this solution method is  $\text{FSM}@c\text{FSM-}L_{cr}$ , which is detailed in [2], and illustrated for an 550S162-43 stud section under axial compression in Figure 6.

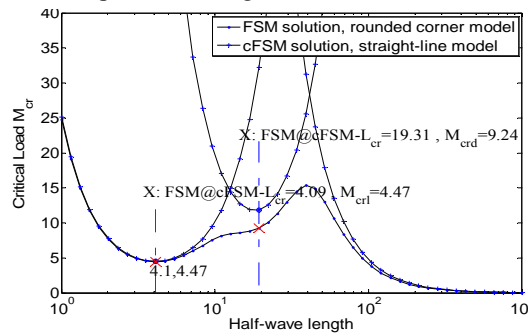


Figure 6 Signature curve augmented with pure mode *c*FSM solution and illustration of the proposed  $\text{FSM}@c\text{FSM-}L_{cr}$  solution

#### ***Application for general boundary conditions***

Modal identification of an FSM solution for general boundary conditions is similar to FEM: at a physical length,  $L$ , the higher modes provide the most direct manner for finding the G, D, and L buckling load or moment. The first identified modes (in ascending buckling values) of G, D, and L can be used as the needed inputs in DSM. For example, critical moment of the 1<sup>st</sup>, 3<sup>rd</sup>, and 10<sup>th</sup> modes in Table 1 may be used as  $M_{cre}$ ,  $M_{crd}$ , and  $M_{cr\ell}$  respectively, and thus as the DSM inputs to predict the bending strength at  $L=108$  in. Moreover, if  $c$ FSM is applicable (no round corners), modal identification can be performed by  $c$ FSM as shown in Table 4. Thus, the engineer can pick the first identified G, D, and L modes, or the modes having the highest individual G, D, and L participation (e.g., the 11<sup>th</sup> or 12<sup>th</sup> modes have more L participation than the 10<sup>th</sup> L mode though the difference in this case is negligible).

Modal decomposition in  $c$ FSM has the ability to decompose the deformation field into individual mode or combined modes of interest. Though the critical loads of pure modes in  $c$ FSM can not be used directly with DSM, the longitudinal terms contributing most to the pure modes can be determined and these terms then used in the conventional FSM solution to force the member to buckle in the desired local or distortional buckling mode. These buckling loads may then be used as DSM inputs to predict the ultimate strength in design. To illustrate consider again the 400S162-68 SSMA stud section at  $L=108$  in. and C-C boundary conditions. The participations for the longitudinal terms in pure local and distortional buckling from  $c$ FSM are provided in Figure 7.

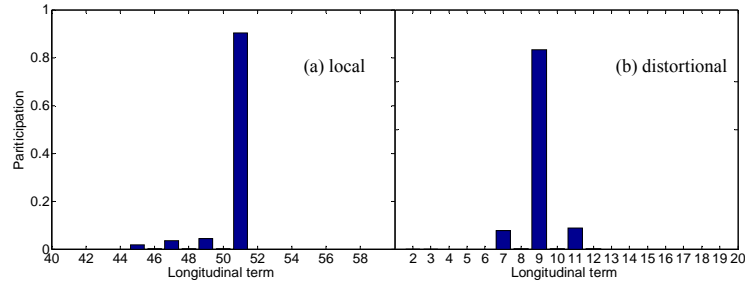
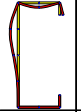
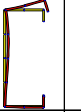
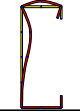
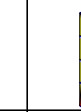




Figure 7 Longitudinal term participation of  $c$ FSM local and distortional buckling

Similar to the two step-procedure for simply supported boundary conditions, first, the pure local and distortional buckling modes are solved by  $c$ FSM (first two columns in Table 5) and the contributed longitudinal terms for each mode are identified (Figure 7). Then, second, the conventional FSM solutions are calculated by using the identified longitudinal terms for each mode (3<sup>rd</sup> and 4<sup>th</sup> columns in Table 5). The conventional FSM solution is successfully restrained

to the desired mode by the identified longitudinal terms, and the critical moments show excellent agreement with those by higher modes of the FSM solution (5<sup>th</sup> and 6<sup>th</sup> columns in Table 5). Hence, these  $M_{cr}$ ,  $M_{crd}$ , together with  $M_{cre}$  (critical global buckling moment) can be used as DSM inputs to predict the ultimate strength.

Table 5 Critical moment of pure and FSM solution with cFSM suggested longitudinal terms

	cFSM solution		FSM solution (1 <sup>st</sup> mode)		FSM solution (higher modes)	
	Local	Dist.	Local	Dist.	Local	Dist.
$M_{cr}$ (kips-in)	170.44	95.90	165.56	89.86	165.58	89.86
Mode shapes						
Longitudinal terms	45, 47, 49, 51	7, 9, 11	cFSM suggested (45, 47, 49, 51)	cFSM suggested (7, 9, 11)	All suggested	All suggested

## Conclusion

The conventional finite strip method combined with the constrained finite strip method provides a powerful tool for exploring cross-section stability in cold-formed steel members. Extensions of the conventional and constrained finite strip method to general boundary conditions are important for their application to general purpose design. The elastic and geometric stiffness matrices are formulated based on new shape functions (series) that correspond to general boundary conditions. The constrained finite strip method for general boundary conditions is briefly described with a summary of the bases available. Examples are provided for conventional as well as constrained finite strip method solutions. The discussed algorithms of both conventional and constrained finite strip method are implemented in the open source stability analysis program: CUFSM. The strength of this new extension to general boundary conditions is demonstrated through the application with the direct strength method in member design.

## Acknowledgements

This paper is based in part upon work supported by the U.S. National Science Foundation under Grant No. 0448707. Any opinions, findings, and conclusions or recommendations expressed in this material are those of the author(s) and do

not necessarily reflect the views of the National Science Foundation. Discussion and collaboration with Sándor Ádány is greatly appreciated.

## References

1. Schafer, B.W. and Ádány, S., *Buckling analysis of cold-formed steel members using CUFSM: Conventional and constrained finite strip methods.*, in *18<sup>th</sup> International Specialty Conference on Cold-Formed Steel Structures: Recent Research and Developments in Cold-Formed Steel Design and Construction*. 2006. p. 39-54.
2. Li, Z. and Schafer, B.W., *Application of the finite strip method in cold-formed steel member design*. Journal of Constructional Steel Research, 2010. 66(8-9): p. 971-980.
3. NAS, *2007 Edition of the North American Specification for the Design of Cold-Formed Steel Structural Members*. 2007, Washington, DC: American Iron and Steel Institute.
4. Li, Z. and Schafer, B.W., *Finite Strip Stability Solutions for General Boundary Conditions and the Extension of the Constrained Finite Strip Method*. in *Trends in Civil and Structural Engineering Computing*. 2009. Stirlingshire, UK: Saxe-Coburg Publications.
5. Li, Z. and Schafer, B.W., *The constrained finite strip method for general end boundary conditions*, in *Structural Stability Research Council - Proceedings of the 2010 Annual Stability Conference*. 2010: Orlando, FL, USA. p. 573-591.
6. Bradford, M.A. and Azhari, M., *Buckling of plates with different end conditions using the finite strip method*. Computers & Structures, 1995. 56(1): p. 75-83.
7. SSMA, *Product Technical Information*, ICBO ER-4943P. 2001, Steel Stud Manufacture Association.
8. Schafer, B.W., Li, Z., and Moen, C.D., *Computational modeling of cold-formed steel*. Thin-Walled Structures, 2010. In Press, Corrected Proof.
9. Ádány, S. and Schafer, B.W., *Buckling mode decomposition of single-branched open cross-section members via finite strip method: Derivation*. Thin-Walled Structures, 2006. 44(5): p. 563-584.
10. Ádány, S. and Schafer, B.W., *Buckling mode decomposition of single-branched open cross-section members via finite strip method: Application and examples*. Thin-Walled Structures, 2006. 44(5): p. 585-600.
11. Ádány, S. and Schafer, B.W., *A full modal decomposition of thin-walled, single-branched open cross-section members via the constrained finite strip method*. Journal of Constructional Steel Research, 2008. 64(1): p. 12-29.
12. Silvestre, N. and Camotim, D., *First-order generalised beam theory for arbitrary orthotropic materials*. Thin-Walled Structures, 2002. 40(9): p. 755-789.
13. Silvestre, N. and Camotim, D., *Second-order generalised beam theory for arbitrary orthotropic materials*. Thin-Walled Structures, 2002. 40(9): p. 791-820.
14. Hancock, G.J., *LOCAL, DISTORTIONAL, AND LATERAL BUCKLING OF I-BEAMS*. ASCE J Struct Div, 1978. 104(11): p. 1787-1798.
15. AISI, *Direct Strength Method Design Guide*. 2006, Washington, DC.